International Journal of Remote Sensing
Vol. 27, No. 14, 20 July 2006, 3079–3086

Taylor & Francis
Taylor & Francis Group

A method for minimising of low frequency and unwrapping artefacts from interferometric calculations

P. ELIAS*†, C. KONTOES†, O. SYKIOTI†, A. AVALLONE‡, S. VAN GORP§, P. BRIOLE§ and D. PARADISSIS¶

†National Observatory of Athens, Institute for Space Applications and Remote Sensing, Metaxa and Vas. Pavlou Str. 15236 Palaia Penteli, Athens, Greece

‡Istituto Nazionale di Geofisica e Vulcanologia, Centro per la Sismologia e Ingegneria Sismica, Via Castello D'Aquino, 83035 Grottaminarda (AV)

§Institut de Physique de Globe de Paris, Departement de Sismologie, 4, place Jussieu, 75252 Paris cedex 05, France

¶National Technical University of Athens, Department of Surveying Engineering, 9 Heroon Polytechniou Str, Zographos, Athens, Greece

(*Received 2 August 2004; in final form 10 January 2006*)

On 7 September 1999 a magnitude M_W=5.9 earthquake occurred in the Athens area of Greece producing a subsidence of 6–7 cm detected by radar interferometry. This study introduces a processing technique, which produces a clear deformation pattern of the earthquake, mostly released from artefacts due to orbital effects, unwrapping cycle slipping errors and atmospherics disturbances. A set of 17 ERS-1 and ERS-2 SAR images acquired between December 1997 and January 2001 has been used. The contribution of each artefact to the interferograms was calculated, both in the frequency and spatial domains.

1. Introduction

Satellite radar interferometry has been employed to assess the surface deformation field caused by geophysical phenomena. It provides invaluable help in earthquake modelling, especially for locating blind seismogenic faults, as in the case of Athens, Greece (figure 1(*a*)) earthquake of 7 September 1999 at 11:56:51 UTC (Kontoes *et al.* 2000).

However, the interferometric calculations suffered from noise interference preventing the earthquake parameters to be assessed precisely. This noise is due to:

- Low frequency artefacts due to atmospheric and orbital effects, with a wavelength larger than ~2 km.
- High frequency artefacts induced by DEM errors, with a wavelength smaller than ~0.2 km.
- Intermediate frequency artefacts due to unwrapping failures, with a typical wavelength of ~1 km (figure 1(*b*)).

The aim of this study was to produce a clear deformation pattern by minimising each one of the low and intermediate frequency artefacts at the level of sub-cycle [−14, 14] mm, while keeping the original phase of each single interferogram intact.

*Corresponding author. Email: pelias@space.noa.gr

International Journal of Remote Sensing
ISSN 0143-1161 print/ISSN 1366-5901 online
http://www.tandf.co.uk/journals
DOI: 10.1080/01431160600578388

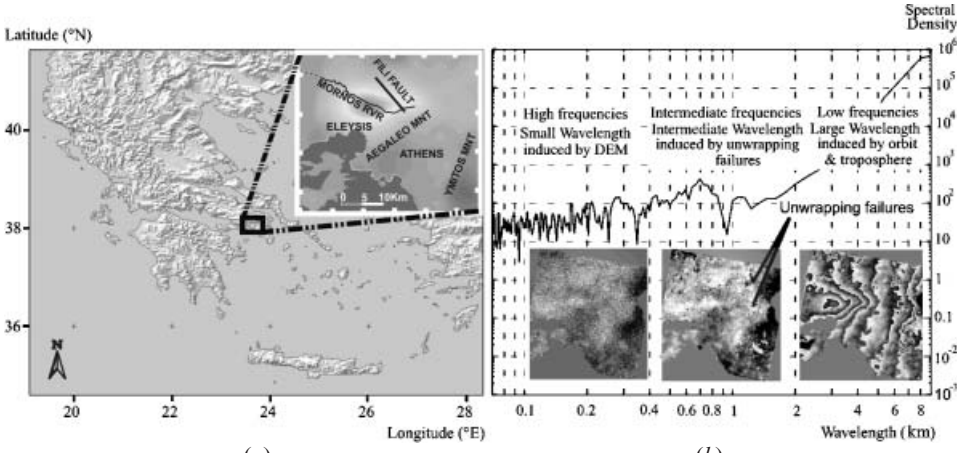

Figure 1. (*a*) The study area. (*b*) The interferometric spectral density along a section crossing the earthquake area. It corresponds to a co-seismic interferogram spanning the period from 19 September 1998 to 9 October 1999.

Note that the high frequency DEM artefacts, calculated as the ratio of the DEM error (10m) over the interferometric 'altitude of ambiguity' (30 m–500 m) (Massonet *et al.* 1998) were all originally below the cycle level (0.3–0.02 cycles). The proposed technique applies stacking, low- (and high-) pass filtering.

2. Data analysis

Seventeen ERS-1 and ERS-2 raw images, acquired before and after the earthquake, spanning the period from December 1997 to January 2001, where used. Eighty-one pre-, co-, and post-seismic interferograms were calculated, using the CNES DIAPASON software. Among them, thirty-one of the most coherent, in time and space, interferograms were used to calculate a collective coherence mask, defined as the average standard deviation of the phase values within a three pixel wide moving window (Chaabane *et al.* 2003). Figure 2 illustrates a time versus baseline diagram of the 81 interferograms, with the thick lines representing the 31 combinations used.

3. Processing step 1: Unwrapping and minimisation of orbital effects

The selected interferograms were unwrapped using the SNAPHU software developed by Chen *et al.* (2000). Initially the orbital effects of the co-seismic interferograms (figures 3(*a*) and 3(*b*)) were minimised as follows. The edges of the interferograms falling far outside the deformation pattern modelled by Kontoes *et al.* (2000) were considered intact by the earthquake. The collective coherence mask was used for selecting and keeping in the calculations only the most coherent pixels located at the edges of the interferograms. The deformation of the pixels at the edges of the interferograms was expected to follow a well-defined *t*-student distribution around a local zero mean. Then, by forcing each local deformation mean to zero, pairs of linear transformations applying to north–south and east–west directions was produced. These linear transformations were used to reassess the interferometric pixel values, resulting in a new set of interferograms on which the orbital fringe effect was minimised as in figures 3(*c*) and 3(*d*). Analysing the phase values on

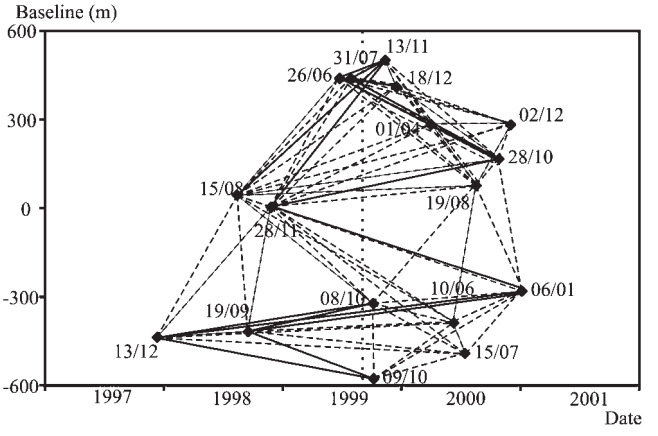

Figure 2. The set of interferometric pairs used in the study. The vertical dotted line indicates the date of the earthquake occurrence. The interferogram samples are located in the study area shown in figure 1(*a*).

the section 'cs' crossing the deformed area in the west–east direction shows that the achieved phase correction reached a maximum level of 25mm (~4 fringes) along the 32 km section length. Figures 3(*c*) and 3(*d*) show the effect of tilting and shifting applied to the plotted phase values. The resulted interferograms are denoted hereafter as 'tilted-shifted' co-seismic interferograms.

4. Processing step 2: Stacking and filtering

The tilted-shifted unwrapped interferograms (figure 3(*d*)) were stacked to obtain a temporal mean deformation field. The stacking technique produced a mean image $S_{i,j}$ defined as:

$S_{i,j}$=mean ($I_1(i,j)$, $I_2(i,j)$, …, $I_n(i,j)$), where I=1, …, K, j=1, …, L, n is the number of interferometric images, K and L denote the size of the images in pixels, and I_m (i, j) is the pixel value at pixel location (i, j).

The stacked image was low pass filtered using a 2 km wide kernel (figure 4). It was considered the best-suited kernel size between the tested ones (1 km, 2 km and 4 km). As shown in figure 5(*a*), illustrating the spectral density of the stacked interferogram along 'cs' (plot (a)), the use of kernel sizes other than 2 km resulted either in excess smoothing (plot (d)) or retention of noise (plot (b)) at intermediate to low frequencies wavelengths. The comparison of plots (a) and (c) shows that the resulted mean approximation of the deformation field is mostly released from high and intermediate frequencies. This deformation field image was used to correct the unwrapping algorithm noise on each single interferogram as follows.

5. Processing step 3: Correction of unwrapping failures

The resulting deformation field of figure 4 was subtracted from each single co-seismic interferogram. This resulted in a set of images where the deformation pattern of the main earthquake was almost eliminated. The different images were affected by artefacts described in figure 1(*b*) (apart from orbital since they were minimised in processing step 1). These images were low pass filtered using a 4 km wide kernel, which resulted in keeping only low frequency variation patterns caused mainly by

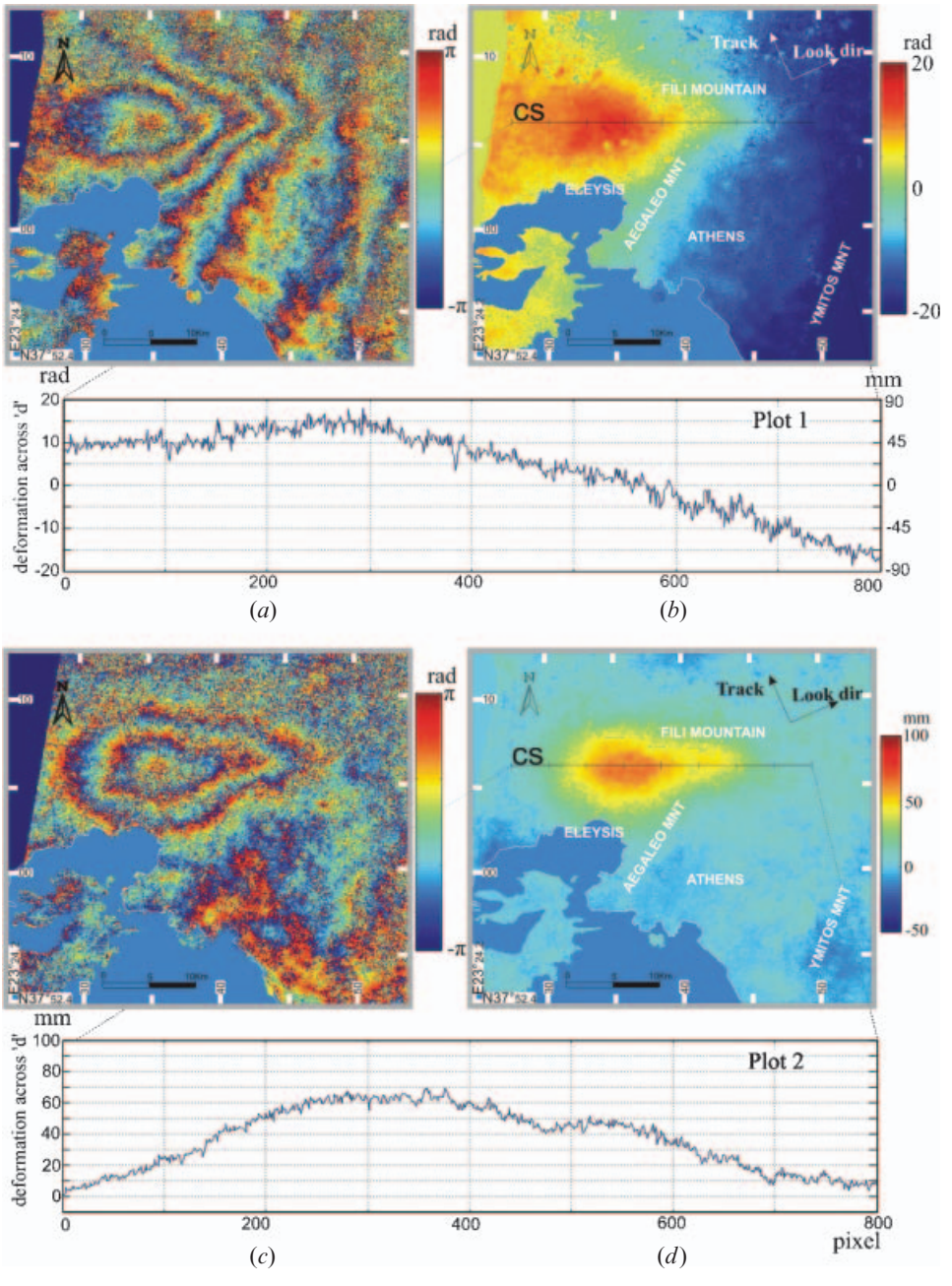

Figure 3. An example demonstrating the effect of tilting-shifting procedure applied on the single interferogram spanning the period from 19 September 1998 to 9 October 1999. (*a*) Initial interferogram calculated by the DIAPASON software. The orbital artefacts are visible. (*b*) The same interferogram after unwrapping using the SNAPHU software. (*c*) The phase interferograms and (*d*) the corresponding unwrapped interferograms after minimization of orbit artefacts. The plot diagrams 1 and 2 show the unwrapped phase values along section 'cs' before and after minimisation of orbit artefacts.

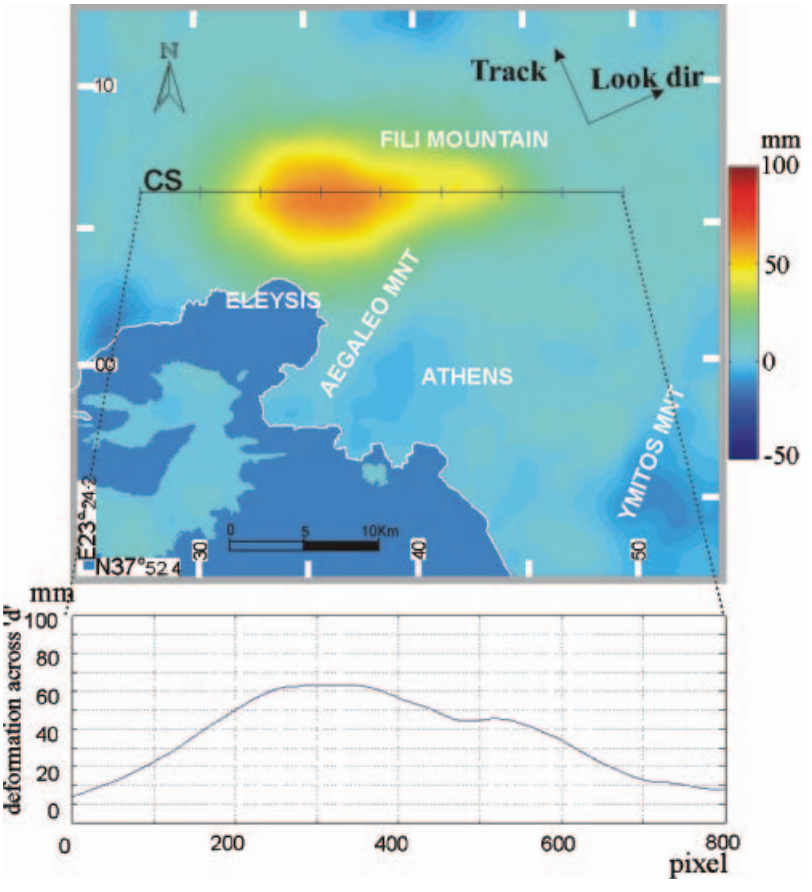

Figure 4. Stacked low pass filtered image.

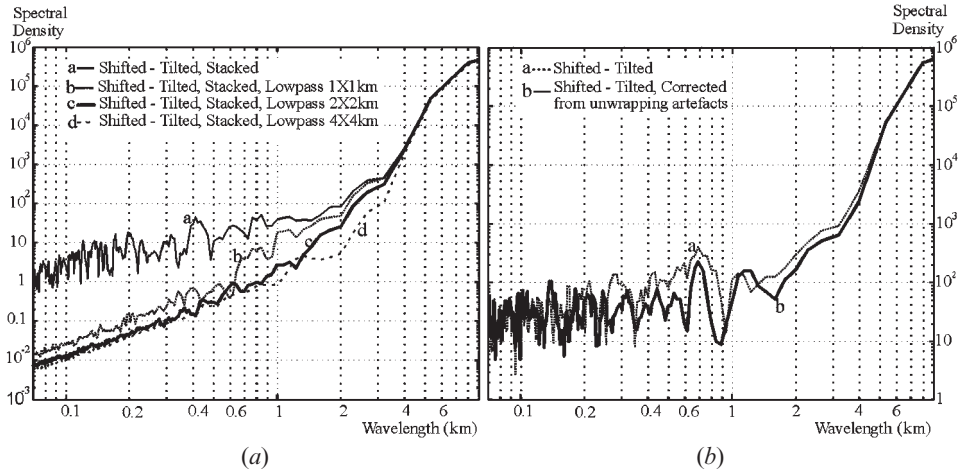

Figure 5. (*a*) The effect of low pass spatial filtering in the frequency domain along section 'cs'. (*b*) The minimisation of unwrapping artefacts in the frequency domain along section 'cs'.

the atmosphere. Several kernel sizes were tested but, examining the corresponding spectral densities, it was evident that the 4 km wide kernel was best suited for removing the intermediate and high frequency patterns. Each of the resulting low frequency images was subtracted from the initial tilted-shifted co-seismic interferograms keeping only the intermediate and high frequency residuals. A simpler processing flow was also tested, rendering quite similar results in the retention of intermediate and high frequency residuals, applying high pass filtering in the frequency domain, instead using spatial convolution. At this processing stage the obtained phase residuals are mostly released by orbital (step 1), earthquake (steps 2 and 3), and atmospheric disturbances (step 3), all being minimised to sub-cycle level [−14, 14] mm. As already mentioned, the high frequency artefacts due to DEM errors were originally below the cycle level attributing only to a very small percentage of the cycle (0.3–0.02 cycles). Therefore the remaining phase residuals exceeding the range of a cycle are due to unwrapping cycle slipping caused by algorithmic calculations. All pixels affected by algorithmic artefacts were identified and their corresponding phase values were shifted by one fringe until within the right cycle level. The improvement is evident when analysing plots (a) and (b) of figure 5(*b*), illustrating the spectral density along the section 'cs' before and after processing of a single interferogram.

6. Validation

Stacking all processed single interferograms resulted in the improved deformation field of figure 6. In order to assess the value of the proposed processing technique, the initial as well as processed single and stacked interferograms were compared with a set of in situ levelling observations, which had been available for the test area before and after the earthquake event. This set comprises of 10 levelling measurements taken along the Mornos river open aqueduct (figure 6) crossing the area (figure 1(*a*)). The National Technical University of Athens, Department of Surveying Engineering, conducted a series of levelling operations from 1984 and 2001 respectively (Kotsis *et al.* 2004). At each levelling point the corresponding elevation values were subtracted, to estimate the aqueduct elevation change due to the earthquake. The accuracy level in the calculations of the elevation change was estimated to be of 4 mm.

The comparison of the elevation changes provided by the corrected interferometric calculations and the in-situ levelling data are shown graphically in figure 7(*a*) and (*b*). The accordance of in situ measurements and the corresponding interferometric estimations after processing is apparent. The improvement of a single unwrapped interferogram, in terms of mean absolute error, was estimated to be of the order of 29.9% of a fringe (figure 7(*a*)) and 30.5% of a fringe for the stacked interferograms (figure 7(*b*)).

7. Conclusions

The proposed technique minimised the orbital effects and the intermediate frequency unwrapping failures from interferometric calculations. The suggested stacking and filtering approach showed a clear deformation pattern of the earthquake, released from the aforementioned artefacts and from atmospheric disturbances. This process does not alter the essential part of the phase values of the initial interferograms and it is completely reversible. The resulted deformation

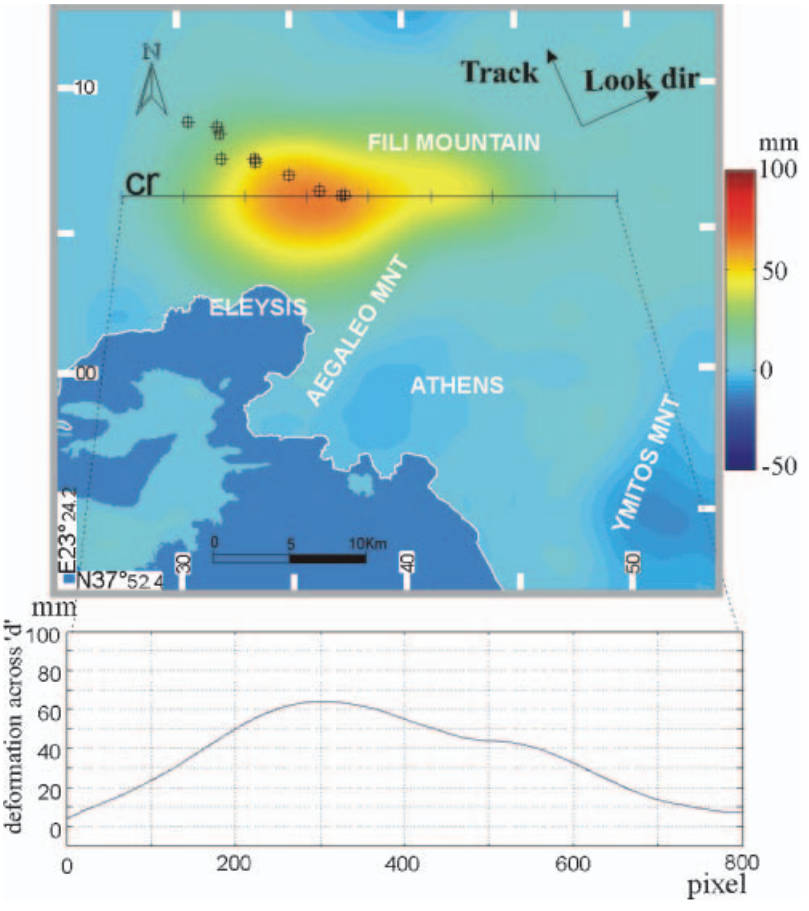

Figure 6. The improved deformation pattern of the earthquake. The cross hair points indicate the locations of the levelling positions along the Mornos river open aqueduct.

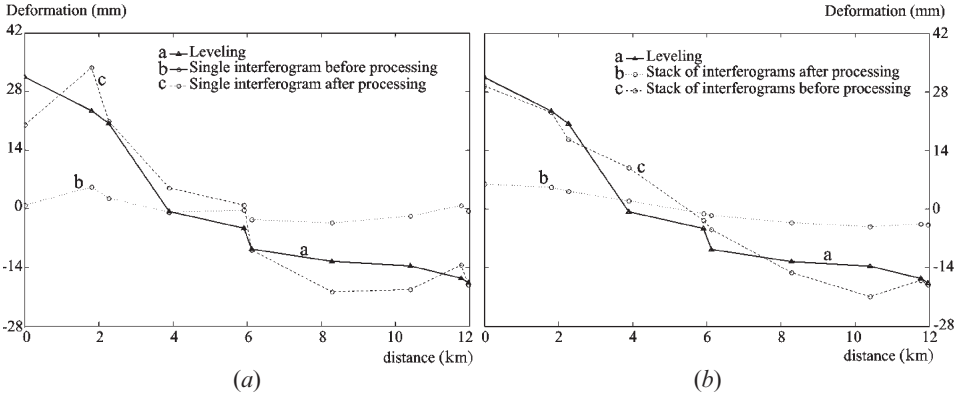

Figure 7. Relative elevation change estimations caused by the earthquake along the Mornos river open aqueduct. The interferometric calculations of the elevation change and the corresponding levelling data are illustrated. Plate (*a*) compares the estimations provided by a single co-seismic interferogram (spanning the period from 19 September 1998 to 9 October 1999) with the in-situ measurements before and after processing. Plate (*b*) shows the same for the stacked interferograms. The accordance of the two data sets is obvious.

products contribute to a more accurate assessment of the deformation source parameters and could be utilised to assess slow rate seismic displacements.

Acknowledgements
We are grateful to the European Space Agency (ESA) for providing ERS-1 and ERS-2 SAR data, in the frame of ESA-GREECE AO project 1489OD/11-2003/72.

References

CHAABANE, F., AVALLONE, A., TUPIN, F., BRIOLE, P. and MAÎTRE, H., 2003, Correction of local and global tropospheric effects on differential SAR interferograms for the study of earthquake phenomena. In *IGARS 2003*, Toulouse, 21–25 July.

CHEN, C.W. and ZEBKER, H.A., 2000, Phase unwrapping for large SAR interferograms: Statistical segmentations and generalised network models. *IEEE Transactions on Geoscience and Remote Sensing*, **40**, pp. 1709–1719.

KONTOES, C., ELIAS, P., SYKIOTI, O., BRIOLE, P., REMY, D., SACHPAZI, M., VEIS, G. and KOTSIS, I., 2000, Displacement field and fault model for the September 7, 1999 Athens earthquake inferred from ERS2 satellite radar interferometry. *Geophysical Research Letters*, **27**, pp. 3989–3992.

KOTSIS, I., KARAMITSOS, S., KONTOES, C., PARADISSIS, D., SYKIOTI, O., ELIAS, P. and BRIOLE, P., 2004, Verifying InSAR derived vertical differential displacements by leveling. Application along the Mornos open aqueduct. *Working Week in Athens*, International Federation of Surveyors, Greece, 22–27 May.

MASSONET, D. and FEIGL, K., 1998, Radar interferometry and its application to changes in the Earth's surface. *Reviews of Geophysics*, **36**, November.